CHEMISTRY OF MATERIALS

Article

pubs.acs.org/cm

Synthesis of Air-Stable CdSe/ZnS Core−Shell Nanoplatelets with Tunable Emission Wavelength

Anatolii Polovitsyn,[†,‡] Zhiya Dang,[†] José L. Movilla,[§] Beatriz Martín-García,[†] Ali Hossain Khan,[†] Guillaume H. V. Bertrand,[†,∥] Rosaria Brescia,[†] and Iwan Moreels*[,†]

[†]Istituto Italiano di Tecnologia, via Morego 30, 16163 Genova, Italy

[‡]Dipartimento di Fisica, Università di Genova, Via Dodecaneso 33, 16146 Genova, Italy

[§]Departamento de Educación, Universitat Jaume I, Av. Vicent Sos Baynat s/n, 12071 Castellón, Spain

Supporting Information

ABSTRACT: In the past few years, several protocols have been reported on the synthesis of CdSe nanoplatelets with narrow photoluminescence (PL) spectrum, high PL quantum efficiency, and short exciton lifetime. The corresponding core/shell nanoplatelets are however still mostly based on CdSe/CdS, which possess an extended lifetime and a strong red shift of the band-edge absorption and emission, in accordance with a quasi-type-II band alignment. Here we report on a robust synthesis procedure to grow a ZnS shell around CdSe nanoplatelets at moderate temperatures of 100−150 °C, to improve the optical properties of CdSe nanoplatelets via a type-I core/shell heterostructure. The shell growth is performed under ambient atmosphere, in either toluene or 1,2-dichlorobenzene. The variation of the shell thickness induces a continuous red shift of the PL peak, eventually reaching 611 nm. The PL quantum efficiency is increased compared to the original CdSe cores, with values up to 60% depending on the shell thickness. High-resolution transmission electron microscopy reveals a bending of the nanoplatelets caused by strain due to 12% lattice mismatch between CdSe and ZnS. The present procedure can easily be translated to other core/shell nanocrystals, such as CdSe/CdS and CdSe/CdZnS nanoplatelets.

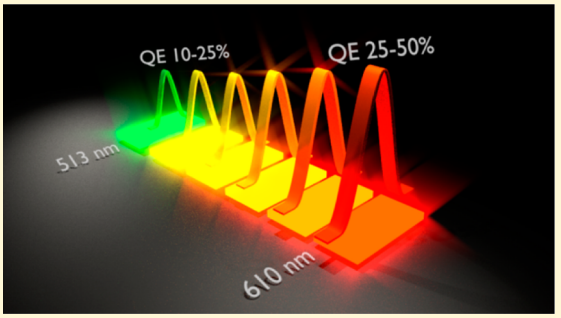

INTRODUCTION

The first syntheses of colloidal semiconductor nanocrystals (NCs) have been published several decades ago.[1−3] Due to their small size, they experience strong quantum confinement in all dimensions and are therefore also referred to as quantum dots (QDs). Already early on, their size- and shape-dependent band structure made them excellent candidates to study exciton dynamics in confined systems,[4−7] and to use them in optoelectronic and photonic applications[8,9] such as light-emitting diodes,[10] solar cells and photodetectors,[11,12] or fluorescent dyes.[13]

Nanometer-sized QDs contain a significant number of surface atoms. The exposure of such a large surface to the environment often leads to oxidation and carrier trapping at the surface, generally leading to a reduced photoluminescence quantum efficiency (PL QE). To prevent this, procedures have been developed to deposit a protective shell of another semiconductor material around the NC core, increasing the PL QE and reducing the contribution of trap states to the electron−hole recombination.[14−17] Starting from a CdSe core, typical materials used for the shell growth are ZnS[14,15] or CdS.[16,17] Depending on the choice of core and shell material, the PL QE and carrier dynamics can be tuned via the lattice mismatch, which for instance plays an important role in the density of interface traps,[18,19] and the valence and conduction bands offset, which determines the extent of carrier delocalization and hence the electron−hole overlap in the final core/shell NCs.[16,17]

To increase the radiative decay rate in semiconductor QDs, recent efforts have been directed at the growth of (quasi-)2D nanoplatelets (NPLs), typically composed of CdSe.[20,21] Narrow PL spectra with full widths at half-maximum (FWHM) of 8−9 nm[20,22] compared to 22−30 nm for CdSe QDs with similar emission wavelength (Supporting Information, SI, Figure S1), a large oscillator strength of the band-edge transition,[20,23,24] and few-nanosecond PL lifetime at room temperature[20] make NPLs suitable for low-threshold amplified emission and lasing,[25−30] quantum emission,[31] and strong light−matter interactions.[32] They have been successfully assembled into long stacks[33] and needles,[34] leading to Förster resonance energy transfer between different NPLs that can occur on a picosecond time scale.[35,36]

NPL heterostructures mainly come in two forms. Core/crown NPLs have extended lateral dimensions after shell growth while maintaining the same thickness as the original

Received: April 12, 2017
Revised: June 11, 2017
Published: June 12, 2017

DOI: 10.1021/acs.chemmater.7b01513
Chem. Mater. 2017, 29, 5671−5680

core, and exist as CdSe/CdS type-I[37,38] and CdSe/CdTe type-II heteroNPLs.[39] However, they leave a large part of their surface area exposed. Core/shell NPLs, with the shell grown on top and bottom facets, can also be synthesized[40,41] and have already demonstrated high PL QEs,[31] a suppressed PL intermittency (blinking),[31] and applications in oxygen sensing[42] or lasing.[28−30] Such NPLs are, with the exception of the CdSe/$Cd_xZn_{1-x}S$ NPLs,[31] typically based on CdSe/CdS, which, due to the small conduction band offset, are in a quasi-type-II regime with a strong electron delocalization and consequently a reduced electron−hole overlap and extended PL lifetime.[30]

Therefore, core/shell NPLs with a type-I band alignment would be highly desirable. Here we report on a novel heat-up procedure to synthesize a ZnS shell around CdSe core NPLs, yielding an improved PL QE compared to the original CdSe NPLs, and increased PL stability of NPL close-packed films under ambient conditions. We used a single-source precursor route based on zinc diethyldithiocarbamate ($Zn(DDTC)_2$), which decomposes at relatively low temperatures in the presence of amine[43−45] so that a synthesis temperature of 100−150 °C could be maintained. The core/shell NPLs are characterized with X-ray diffractometry, transmission electron microscopy (TEM), and optical spectroscopy. Growing the shell with different precursor concentrations leads to a continuously tunable band-edge absorption and PL, with an emission that is red-shifted from 508−514 nm up to 593−611 nm, depending on the initial core dimensions and final ZnS shell thickness. This trend is confirmed by *k·p* calculations, which highlight that the 2D NPL shape leads to a significant reduction of the electron and hole self-energy after ZnS shell growth, yielding a stronger red shift of the band edge compared to CdSe/ZnS QDs.

EXPERIMENTAL SECTION

Materials. Zinc chloride ($ZnCl_2$, 99.999%), cadmium nitrate tetrahydrate ($Cd(NO_3)_2$, 99.997%), cadmium(II) acetate (99.995%), sodium diethyldithiocarbamate trihydrate (99%), zinc diethyldithiocarbamate ($Zn(DDTC)_2$, 97%), carbon disulfide (CS_2, 99.9%), sodium sulfide (Na_2S), oleic acid (90%), oleylamine (70%), didodecyldimethylammonium bromide (DDAB, 98%), formamide (FA, 99.5%), hexane (≥95%), toluene (99.7%), 1.2-dichlorobenzene (DCB, 99%), acetonitrile (99.8%), ethanol (≥99.8%), and methanol (99.9%) were purchased from Sigma-Aldrich. *N*-Trioctylphosphine (TOP, 97%) and cadmium oxide (99.999%) were purchased from Strem Chemicals.

$Cd(DDTC)_2$ Preparation. Two millimolar sodium diethyldithiocarbamate was dissolved in 5 mL of methanol and added at room temperature to a 5 mL solution containing 1 mM $Cd(NO_3)_2$ in methanol while stirring. A white precipitate of cadmium diethyldithiocarbamate ($Cd(DDTC)_2$) formed, which was collected by centrifugation at 5500 rpm, rinsed three times with methanol, and dried at 60 °C for 12 h.

ZnS Shell Growth in Toluene. First, CdSe core NPLs were synthesized according to previously reported procedures (synthesis with dry Cd-acetate).[46] In a typical shell growth, for instance targeting a four monolayer (ML, 1 ML is taken as 0.31 nm) ZnS shell, a 200 μL, 2.26 μM,[47] hexane solution of CdSe NPLs (sample 1) was loaded in a 5 mL vial together with 2 mL of toluene. Next, 20 μL of a mixture of 0.5 M $ZnCl_2$ in oleylamine (preheated to 50 °C), 20 μL of TOP, 2 μL of CS_2, and 3.5 mg of $Zn(DDTC)_2$ were added. The vial was placed on a hot plate at 110 °C (as measured with a thermocouple inserted in a reference solution), with the solution being stirred gently. After approximately 1 h, the sample was cooled to room temperature and subsequently precipitated and redispersed three times, using 2 mL of acetonitrile or methanol as nonsolvent and centrifuging the sample at 5500 rpm for 3 min. Finally the core/shell NPLs were suspended in hexane. In case of significant conucleation of small ZnS clusters (SI, Figure S2), we used *n*-isopropanol to precipitate the sample and 2 min of sonication to redisperse the NPLs. After that we precipitated the NPLs again by centrifugation at 3000 rpm for 30 min and finally redispersed the NPLs in hexane. To obtain different ZnS shell thicknesses, we varied the amounts of injected precursors. For instance, 100 μL of a mixture of 0.5 M $ZnCl_2$ in oleylamine (preheated to 50 °C), 100 μL of TOP, 10 μL of CS_2, and 16 mg of $Zn(DDTC)_2$ can be used to target a 12 ML ZnS shell.

ZnS Shell Growth in DCB. To obtain a thicker ZnS shell, we performed the synthesis in DCB at a temperature of 150 °C. Here we describe a typical procedure, to target a ZnS shell of 14 ML. Other thicknesses can be obtained by injecting different amounts of precursors. CdSe NPLs dispersed in hexane were mixed with DCB at room temperature and subsequently heated under ambient atmosphere on a hot plate. When the temperature of CdSe NPLs (200 μL at 2.26 μM[47] for sample 1) in DCB reached 150 °C, we injected with a syringe pump a mixture of 120 μL of 0.5 M $ZnCl_2$ in oleylamine (preheated to 50 °C), 120 μL of TOP, 12 μL of CS_2, and 20 mg of $Zn(DDTC)_2$ dissolved in 1 mL of DCB. The injection rate was set at 1 mL/h. After synthesis, we used the same purification procedure as described for the toluene-based synthesis.

CdS Shell Growth in Toluene and DCB. To grow a 6 ML CdS shell, a 200 μL, 2.26 μM,[47] hexane solution of CdSe NPLs (sample 1) was loaded in a 5 mL vial together with 2 mL of toluene. Next, 35 μL of a mixture of 0.5 M $CdCl_2$ in oleylamine (preheated to 100 °C), 35 μL of TOP, 3.5 μL of CS_2, and 7.0 mg of $Cd(DDTC)_2$ were added. The vial was placed on a hot plate at 110 °C with the solution stirred gently. After approximately 1 h, the sample was cooled to room temperature and subsequently precipitated as described above. Finally the NPLs were dissolved in hexane.

CdZnS Shell Growth in DCB. To obtain a CdZnS shell, we performed the synthesis in DCB at a temperature of 150 °C. When the temperature of CdSe NPLs (200 μL at 2.26 μM, sample 1) in DCB was established, we injected, with a syringe pump, a mixture of 120 μL of 0.5 M $ZnCI_2$ in oleylamine (preheated up to 50 °C), 120 μL of TOP, 12 μL of CS_2, and 20 mg of $Cd(DDTC)_2$ dissolved in 1 mL of DCB. The injection rate was set at 1 mL/h. After the shell growth, the samples were purified as described above.

c-ALD Growth of ZnS and CdS Shells. CdSe/ZnS core/shell NPLs were synthesized at room temperature using colloidal atomic layer deposition (c-ALD).[41] Two hundred microliters of CdSe NPLs (concentration of 2.6 μM)[47] dispersed in hexane was mixed with 1 mL of toluene. Next 1 mL of a 0.1 M solution of Na_2S in FA was added. The two-phase mixture was vigorously stirred for 15 min to transfer the NPLs to FA. Then the CdSe-S NPLs were precipitated with ethanol and centrifuged at 5500 rpm. After redispersion in 1 mL of FA, 1 mL of a 0.1 M solution of DDAB in toluene was added, and the solution was stirred for 15 min to transfer the NPLs from FA to toluene. The NPLs were precipitated again with ethanol and redispersed in toluene. To deposit a layer of zinc, we injected 10 μL of a preheated 0.5 M $ZnCl_2$ solution in oleylamine and stirred for 20 min. Finally, the CdSe/ZnS NPLs were precipitated with acetonitrile and redispersed in hexane. The procedure above was repeated until the desired number of layers was obtained, and the NPLs were finally dispersed in hexane.

CdSe/CdS core/shell NPLs were synthesized with room temperature c-ALD.[41,42] The first sulfur layer was added by transferring 300 μL of CdSe NPLs (concentration of 1 μM)[47] from hexane to 1 mL of FA, to which 100 μL of Na_2S (0.5 M) was added. After phase separation the polar solution was isolated. Ethanol was added to precipitate the NPLs. After centrifugation at 6000 rpm for 1 min, the precipitate was recovered and dried with nitrogen. Next, NPLs were redispersed in 1 mL of FA. The precipitation was repeated in order to remove excess sulfur. To grow the first layer of cadmium, 1 mL of a 0.5 M cadmium acetate solution in FA was added, and the solution stirred for 1 h. The NPL dispersion was purified as described above, and the NPLs were redispersed in 1 mL of FA. The procedure was repeated until we reached the desirable shell thickness. The final core/shell NPLs were dispersed in 2 mL of toluene with the addition of 180−250

DOI: 10.1021/acs.chemmater.7b01513
Chem. Mater. 2017, 29, 5671−5680

μL of cadmium oleate (0.5 M solution in oleic acid) to stabilize them. Excess oleic acid and cadmium oleate were removed by precipitating the NPLs with acetonitrile, centrifugation, and redispersion in toluene.

Structural Characterization. X-ray diffraction (XRD) analysis was performed on a PANanalytical Empyrean X-ray diffractometer equipped with a 1.8 kW CuKα ceramic X-ray tube, PIXcel^{3D} 2 × 2 area detector and operating at 45 kV and 40 mA. Samples for the XRD measurements were prepared in a glovebox by dropping a concentrated NPL dispersion onto a miscut silicon substrate. The diffraction patterns were collected using Parallel-Beam (PB) geometry and symmetric reflection mode.

Conventional TEM images were acquired on a JEOL JEM-1011 microscope equipped with a thermionic gun at 100 kV accelerating voltage. Samples were prepared by dropping NPL suspensions onto carbon film-coated 200 mesh copper grids. The high resolution TEM (HR-TEM) images were acquired on a 200 kV TEM microscope (JEOL JEM-2200FS) equipped with a spherical aberration corrector (CEOS) for the objective lens, an in-column image filter (Ω-type). Samples were prepared by dropping NPLs suspensions onto holey carbon film-coated 400 mesh copper grids. High-angle annular dark-field scanning transmission electron microscope (HAADF-STEM) images were collected to measure the NPL shell thickness on 8−26 core/shell NPLs. We performed three−four measurements of the thickness along the core/shell NPLs to account for shell thickness variation. A Bruker Quantax 400 energy dispersive X-ray spectrometry (EDS) system with an XFlash 5060 detector was used for the elemental analysis. The EDS elemental maps of NPLs shown are for the Cd Lα, Se Kα, Zn Kα, and S Kα lines, respectively. Geometric phase analysis (GPA) revealed the variation in the periodicities of the HR-TEM contrast via analysis of the local components in the Fourier transform of the image.[48] This method was applied to HR-TEM images of core/shell NPLs, and by selecting an "unstrained" core area in the HR-TEM image as reference, we rendered a mean dilation map.

NMR Analysis. ^{1}H nuclear magnetic resonance (NMR) spectra were recorded on a Bruker Avance III 400 NMR spectrometer, equipped with a BBI inverse probe and Z-gradients, using deuterated solvents. Toluene-d_8 (99.96% atom D, 1 mL vial) and chloroform-$CDCl_3$ (99.96% atom D, 1 mL vial) were supplied by Sigma-Aldrich. The data analysis was performed using MestReNova software version 7.1.

Optical Characterization. Absorbance spectra were recorded using a Varian Cary 3000 UV−vis spectrophotometer. Steady-state and time-resolved PL emission spectra were measured using an Edinburgh Instruments FLS920 spectrofluorometer. The steady-state PL was collected by exciting the samples at 390 nm with a xenon lamp. The PL decay traces were recorded by exciting the samples at 405 nm using a 50 ps laser diode at a repetition rate of 0.05−1 MHz, to ensure complete decay of the emission between the excitation pulses. The data were collected at the PL peak position with an emission bandwidth of 10 nm. PL QE measurements were performed with an integrating sphere.

***k·p* Calculations.** The NPL ground excitonic states were obtained by solving the corresponding 3D effective mass Schrödinger equation (see also SI, section theoretical outline). The Hamiltonian takes into account: (i) the anisotropy of the effective masses and their dependence on the NPL thickness;[49] (ii) finite core/shell conduction and valence band offsets allowing for exciton leakage into the shell; (iii) different core and shell effective masses; and (iv) the single- and two-particle Coulomb interaction terms stemming from the dielectric mismatch between the NPLs and the organic ligands.[50] The variational wave function describing the exciton reads $\Psi(r_e r_h) = Nc(r_e)c(r_h)\, e^{-\alpha[(x_e-x_h)^2+(y_e-y_h)^2]}$ with $c(r_i) = \cos(k_x x_i).\cos(k_y y_i).\theta_i(z_i)$. In these equations, N is a normalization factor, $k_x = \pi/L_x$, $k_y = \pi/L_y$ (L_x and L_y being the in-plane dimensions of the NPLs), and α is the variational parameter to optimize. The transversal (z) components of the electron and hole wave functions θ_i were obtained numerically by means of a finite differences scheme. SI, Table S1, summarizes the values of the parameters employed in the calculations. To confirm the robustness of the results, we verified their dependence on moderate variations of the main parameters involved. By way of example, a variation of the CdSe/ZnS band offsets from 1.44 eV (electrons) and 0.6 eV (holes) to 1.04 and 1.0 eV (variation of −28% and +67%, respectively) increased (decreased) the estimated red shift (the electron−hole overlap) by no more than 6%.

RESULTS AND DISCUSSION

The ZnS shell growth is demonstrated on CdSe NPLs that emit around 515 nm, which are ca. 1.2 nm thick[25] (SI, Figure S3). As a starting point for the ZnS shell formation, we added 10−50 μL of a 0.5 M $ZnCl_2$ solution in oleylamine and 1−5 μL of CS_2 to a dispersion of 200 μL of 2.26 μM CdSe NPLs in toluene (starting from CdSe sample 1, SI, Figure S3). When heating this mixture up to 110 °C under ambient (open air) conditions, CS_2 reacts with oleylamine yielding thiocarbamic acid, which in the presence of Zn-ions forms a Zn-thiocarbamate salt.[51] The *in situ* formed single-source precursor then decomposes, which can occur already at temperatures around 50−80 °C,[43−45] and forms a layer of ZnS around the CdSe NPLs. After shell growth, the band-edge absorption and PL spectra show a red shift of 60 nm (Figure 1 and SI, Figure S4). Note that similar, yet smaller

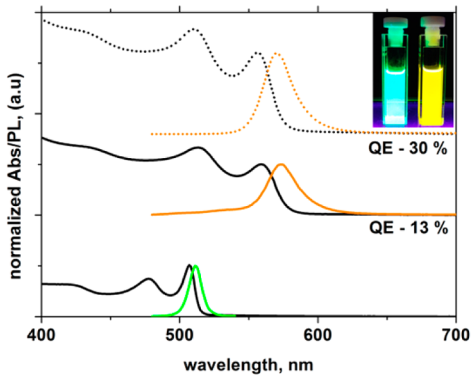

Figure 1. Absorbance and photoluminescence spectra for CdSe and CdSe/ZnS core/shell NPLs. Bottom (full lines): Spectra of the original CdSe core NPLs (sample 1). Middle (full lines): Spectra of CdSe/ZnS NPLs that are synthesized from a zinc oleyl-carbamic precursor produced in situ. The PL QE (λ_{ex} = 390 nm) equals 13%. Top (dashed lines): Spectra of CdSe/ZnS NPLs, with a ZnS shell obtained with $Zn(DDTC)_2$. The PL QE has increased to 30%. Inset: Photo image of CdSe NPLs (left) and CdSe/ZnS core/shell NPLs (right, synthesized with $Zn(DDTC)_2$), both suspended in hexane under 365 nm UV illumination.

red shifts have been observed previously with CdSe/ZnS QDs,[14] CdS/ZnS QDs,[44] and CdSe NPLs passivated with Zn-oleate,[52] supporting the formation of the ZnS shell.

Instead of relying solely on the *in situ* generation of single-source precursors, improved results were obtained when we replaced 50 mol % of CS_2 and $ZnCl_2$ with an equivalent amount (calculated based on the Zn-concentration) of $Zn(DDTC)_2$. The inclusion of this short-chained precursor yielded a similar PL spectral position of 571 nm after ZnS shell growth, yet with sharper band-edge absorption and PL features, and a higher PL QE, which increased from 13% for the first procedure to 30% when using $Zn(DDTC)_2$ (Figure 1).

The role of the precursors was further investigated with ^{1}H NMR spectroscopy. First, as already mentioned, CS_2 reacts with oleylamine to form a dithiocarbamic acid, which yields the S-precursor for the shell growth. Indeed, after mixing equimolar amounts of oleylamine and CS_2, specific resonances at 3.7 and

DOI: 10.1021/acs.chemmater.7b01513
Chem. Mater. 2017, 29, 5671−5680

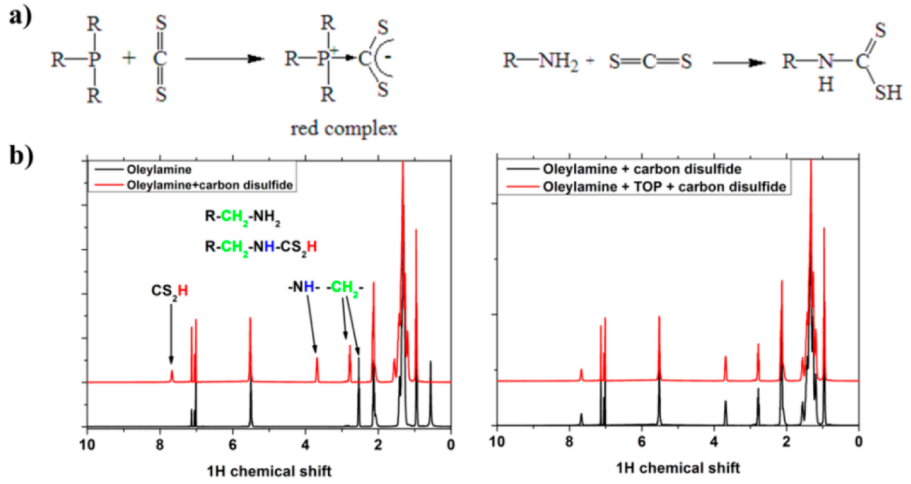

Figure 2. (a) Scheme of the chemical interactions between oleylamine, TOP, and CS_2. (b) ^1H NMR spectra of oleylamine/CS_2 (left) and oleylamine/TOP/CS_2 mixtures (right).

7.6 ppm appear that correspond to the −NH− and − SH protons, respectively (Figure 2). In addition, CS_2 is a volatile species. However, as indicated by the saturated red color of a solution, obtained after mixing CS_2 and TOP (SI, Figure S5), these two chemicals form a phosphorus−carbon ylide complex.[53] After addition of oleylamine, the solution again becomes transparent within 15 min, and the ^1H NMR spectrum confirms the formation of dithiocarbamic acid (Figure 2). As the chemical shift of all NMR peaks is comparable to the first case, we can conclude that TOP serves to form an intermediate complex with CS_2, which can reduce the loss of CS_2 due to evaporation during synthesis, while it does not alter the formation of the final dithiocarbamic acid.

To further confirm that every precursor is required for core/shell NPLs with high and stable PL QE, we also systematically excluded each of them during the ZnS shell growth. We targeted a deposition of 4 ML of ZnS, growing the shell via the $Zn(DDTC)_2$-based heat-up reaction in toluene at 110 °C. We started from CdSe NPL sample 1, and the reaction proceeded for 1 h as described above. We dropcasted the resulting CdSe/ZnS NPLs as a close-packed thin film onto a glass substrate, and examined their optical stability under ambient conditions for 60 days by monitoring the PL under UV illumination (Figure 3a). Absorption and PL spectra were collected on the corresponding solutions (Figure 3b). When excluding $ZnCl_2$ or TOP, we observed a PL red shift to only 544 and 561 nm, respectively, which indicates the growth of a thinner layer of ZnS around CdSe NPLs compared to the full procedure. In absence of CS_2 the first excitonic peak shifted to 560 nm; hence, the oleyl-carbamic acid precursor is not necessary to grow a thick shell. However, we did not detect any fluorescence, suggesting poor surface passivation of the latter sample possibly due to the absence of long-chained ligands. Finally, it is clear that the ZnS shell is most stable when it is deposited including all precursors. The red shift upon shell growth is highest in this case, reaching 567 nm, and the close-packed thin films did not show any significant decay of the PL upon storage of the samples for 60 days.

The ZnS shell thickness can be varied by performing the shell growth with different concentration of Zn- and S-precursors (Figure 4). Targeting a given shell thickness between 2 and 14 ML, we mixed the corresponding precursors at room temperature with a 2.26 μM CdSe NPL dispersion in toluene

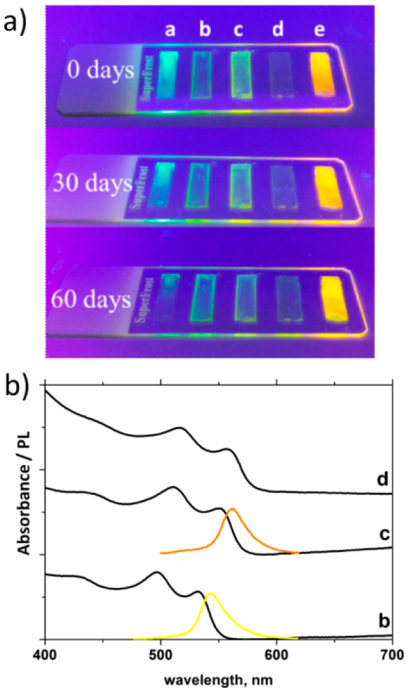

Figure 3. (a) Photo image of close-packed thin films of CdSe (sample 1, shown as film a) NPLs with a targeted 4 ML ZnS shell, synthesized with the heat-up procedure in toluene. In each core/shell NPL synthesis, one component (b, $ZnCl_2$; c, TOP; d, CS_2) was excluded. The full synthesis corresponds to the right-most film (e). The PL was monitored over time when storing the samples under ambient conditions. The CdSe/ZnS sample that was synthesized using all precursors (film e) clearly shows the largest red shift (yellow emission), and the highest optical stability after storage for 60 days. (b) Absorbance and photoluminescence spectra of the corresponding samples (with exclusion of b, $ZnCl_2$; c, TOP; d, CS_2). In the latter case, no PL was measured.

and heated the reaction again to 110 °C. For instance, to grow a 2 ML (14 ML) ZnS shell around 36.5 nm by 10 nm CdSe NPLs (sample 1), we added 30 μL (150 μL) of a 0.5 M $ZnCl_2$ solution in oleylamine, 30 μL (150 μL) of TOP, 2.5 μL (10 μL) of CS_2, and 2 mg (100 mg) of $Zn(DDTC)_2$. We used a larger relative amount of $Zn(DDTC)_2$ when increasing the targeted ZnS shell thickness, to be able to maintain a low concentration

DOI: 10.1021/acs.chemmater.7b01513
Chem. Mater. 2017, 29, 5671−5680

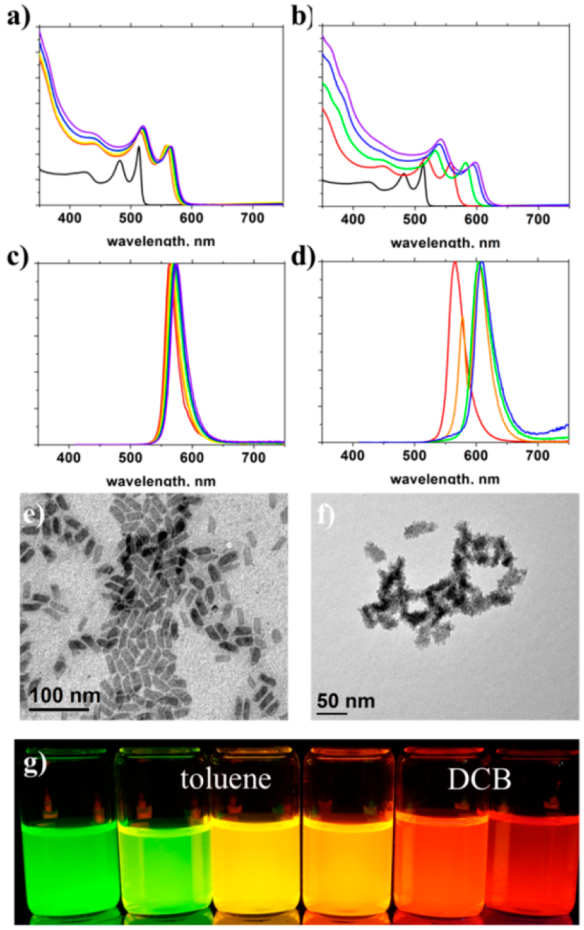

Figure 4. (a,b) Absorbance spectra for CdSe and CdSe/ZnS core/shell NPLs synthesized in toluene (a) and 1,2-dichlorobenzene (DCB) (b). (c,d) Photoluminescence spectra for CdSe/ZnS core/shell NPLs synthesized in toluene (c) and DCB (d). (e) TEM image of typical core/shell NPLs synthesized in toluene. (f) TEM image of core/shell NPLs with (targeted) 14 ML of ZnS shell synthesized in DCB. (g) Image of different samples under UV illumination, from CdSe core (sample 1, green) to CdSe/ZnS core/shell NPLs with increasing ZnS shell thickness synthesized in either toluene (samples 2−4) or DCB (samples 5−6).

of volatile CS_2 during shell growth when growing a thicker ZnS shell. The final core/shell NPLs yielded a tunable PL, with a maximal shift of 60 nm, depending on the concentration of Zn and S added (Figure 4a,c).

Still, toluene limits the growth temperature, thus possibly the ZnS conversion yield, as it has been demonstrated that higher growth temperatures benefit the $Zn(DDTC)_2$ decomposition.[44] Therefore, to further increase the shell ZnS thickness we performed the synthesis in DCB and raised the temperature to 150 °C. To avoid separate nucleation of ZnS, we first heated the NPLs to the final growth temperature, after which we injected the precursors continuously by syringe pump over the course of 1 h. We used the same precursors as for the heat-up synthesis in toluene, now dissolved in DCB (see Experimental Section). With this approach, we were able to red shift the PL peak position by almost 100 nm, to 611 nm, when we targeted a ZnS shell thickness of 14 ML (Figure 4b,d). Further analysis of the optical spectra revealed that the PL FWHM is slightly larger after shell growth, with values of 20−23 nm compared to 9 nm for CdSe core-only NPLs (Figure S3).

TEM images showed that, when using toluene as the reaction medium, the final CdSe/ZnS NPLs preserve their original shape (Figure 4e). However, when growing a thicker ZnS shell in DCB, the final core/shell NPLs had a slightly more irregular shell (Figure 4f). A series of samples synthesized in DCB with different targeted shell thickness was imaged by HAADF-STEM and confirmed the irregular shell growth (SI, Figure S6), possibly induced by strain at the core/shell interface preventing epitaxial growth for thicker ZnS layers. From the average thickness we estimated a typical conversion yield, of precursors into ZnS shell, of 37%, yielding an average thickness about half of the targeted value.

As a consequence of the continuous shift of the PL peak, the CdSe/ZnS core/shell NPLs demonstrate a wide emission color range from 560 nm for a thin ZnS shell, up to 611 nm for the thickest ZnS shell (Figure 4g). To evaluate the PL QE, we also prepared two series of CdSe/ZnS NPLs with a targeted shell thickness up to 11 ML following the continuous injection in DCB. The PL QE increases first to values of about 60% for a targeted 3−5 ML ZnS shell, followed by a monotonic decrease when the shell thickness grows larger (SI, Figure S7, Table S2). This is likely correlated with the increase in surface roughness introduced in samples with a thicker ZnS shell, leading to a larger defect density.

A more detailed investigation of the CdSe/ZnS core/shell NPLs was performed with HR-TEM, HAADF-STEM, and XRD. Zero-loss filtered HR-TEM images of core−shell NPLs with a thin shell (synthesized in toluene with a target thickness of 6 ML) and with a thick shell (synthesized in DCB with a target thickness of 14 ML) are shown in Figure 5a,c, respectively. From HAADF-STEM images of few upstanding NPLs (e.g., Figure 5e), we measured that in toluene the synthesis yields only a 2 ± 0.5 ML shell. In contrast, the shell obtained in DCB is much thicker (SI, Figure S6); in this particular case we even obtained 16 ± 2 ML of ZnS. Here the experimental shell thickness exceeded the target value; however, considering the increased variation in shell thickness along the NPL surface, as was already apparent from the conventional TEM image (Figure 4f), we may slightly overestimate the shell thickness.

The fast Fourier transform (FFT) of core and shell regions show that the crystal phase is cubic for both CdSe and ZnS (Figure 5a,c), with an epitaxial relationship between core and shell, except for the outer domains of the thick-shell sample that are polycrystalline. The XRD pattern for CdSe NPLs (Figure 5f) confirms the zinc blende crystal phase, with characteristic peaks of CdSe at 25.2° ({111} plane), 41.4° ({220} plane), and 49.2° ({311} plane), at slightly smaller angles compared to bulk CdSe, suggesting a 1.5% lattice dilation.[54] After deposition of 2 ML of ZnS shell, the CdSe/ZnS NPLs yielded XRD peaks for the CdSe core region that are shifted to 26.7°, 44.7°, and 52.7°, respectively, implying a 4.9% lattice contraction following shell growth due to compressive strain of the ZnS shell. The peaks that can be associated with the ZnS shell region occur at angles of 28.7°, 47.6°, and 56.2°, respectively, which agree with bulk ZnS. The absence of lattice dilation is possibly due to the larger bulk modulus of ZnS compared to CdSe.[55]

The large lattice mismatch between CdSe and ZnS is further highlighted by GPA (Figure 5b,d) of the HR-TEM images. By selecting an area in the core CdSe region in the HR-TEM image as a reference, the mean dilation maps clearly reveal the core−shell structure, with the CdSe region corresponding to

DOI: 10.1021/acs.chemmater.7b01513
Chem. Mater. 2017, 29, 5671−5680

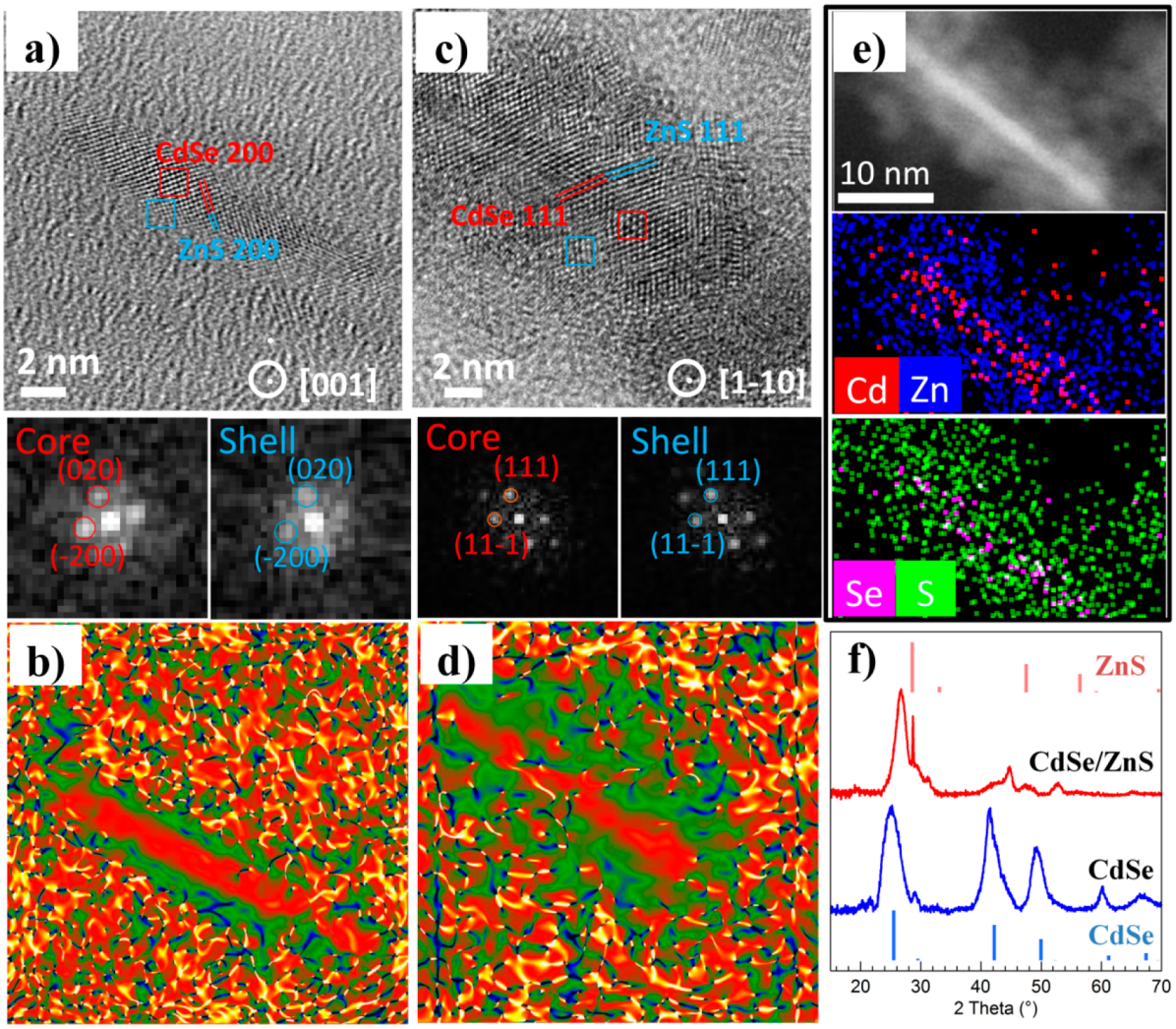

Figure 5. (a) HR-TEM image of CdSe/ZnS NPLs with a 0.6 ± 0.2 nm (2 ± 0.5 ML) shell, oriented with [001] zone axis, and FFT of core and shell region (boxed areas), respectively. (b) Mean dilation map obtained by the GPA method for the same image. (c) HR-TEM image of CdSe/ZnS NPLs with a 5 ± 1 nm (16 ± 2 ML), shell oriented with [1$\bar{1}$0] zone axis, with FFT of core and shell region (boxed area), respectively. (d) Mean dilation map for the same image. (e) HAADF-STEM image and corresponding EDS map for the CdSe/ZnS sample shown in panels c and d. (f) XRD patterns for CdSe core (sample 1) and corresponding CdSe/ZnS NPLs with 2 ML shell. Both core and core/shell NPLs have a cubic crystal lattice. Vertical lines indicate the positions for bulk CdSe (blue) and ZnS (red).

the red area and the ZnS shell shown in green. Note that in these measurements the relative dilation (−12% in the green area relative to the central area) is more closely matched with the lattice mismatch between bulk CdSe and ZnS (12.1%, considering a_{CdSe} = 6.05 Å, ICSD card 620439, and a_{ZnS} = 5.32 Å, ICSD card 41985). We also did not observe significant diffusion of atoms across the CdSe/ZnS interface. Indeed, taking the CdSe/ZnS with a 16 ML shell, the distribution of the elements in the NPLs was mapped using EDS in Figure 5e. The EDS elemental maps confirm the GPA results of the HR-TEM images, with Cd and Se concentrated in the core region, while Zn and S are distributed more evenly. Note that the latter is expected for a side-view of core/shell NPLs even in absence of Zn and S diffusion into the core, as we probe a significant part of the shell when viewing the central region.

As already shown in Figure 4, by increasing the concentration of Zn- and S-precursors, the CdSe/ZnS core/shell NPLs yielded a strong red shift of the PL position. To gain more insight into the nature of this shift, we monitored the evolution of the PL properties by taking aliquots during a shell growth in toluene at 110 °C (SI, Figure S8a). For this reaction, we targeted a final ZnS thickness of 4 ML. We observed a rapid increase of the spectral position of the heavy-hole−electron transition to 547 nm after 10 min, followed by a more gradual shift in the subsequent 50 min, reaching finally 566 nm. For comparison, we also performed a room-temperature synthesis of CdSe/ZnS NPLs using c-ALD. The PL QE of such samples is lower in our case, with typical values of 0.5−4% (SI, Figure S9); however, the room temperature growth in sequential steps yields more control over the final shell thickness. The initial shift observed in toluene at 110 °C coincides with a 542 nm peak observed when 1 ML of ZnS is deposited using c-ALD (SI, Figure S8b). Again, a further shift is observed when adding up to 10 ML of ZnS (Figure 6, black squares, and SI, Figure S9), yielding a final red shift of 82 nm. The shift obtained for c-ALD agrees well with the shift of the CdSe/ZnS core−shell NPLs synthesized at higher temperature (Figure 6, blue triangles). As the c-ALD is executed at room temperature and the red shift in our procedure and the c-ALD are comparable, significant effects due to interface alloying can be

DOI: 10.1021/acs.chemmater.7b01513
Chem. Mater. 2017, 29, 5671−5680

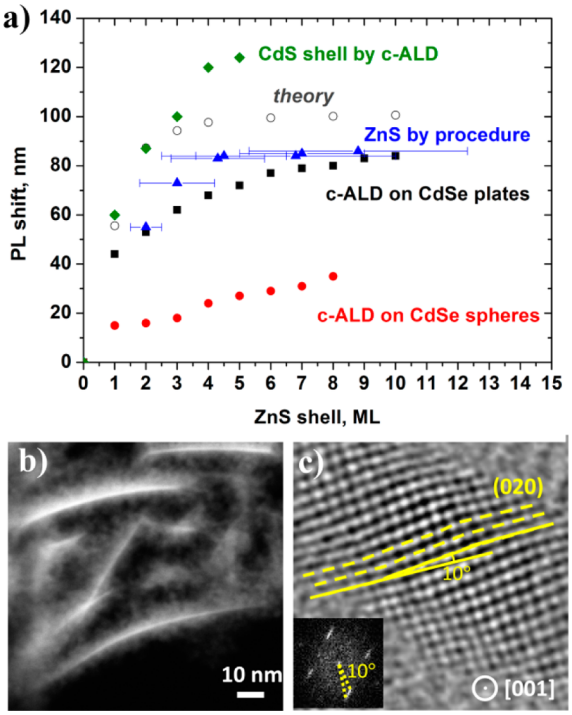

Figure 6. (a) Photoluminescence red shift for CdSe/ZnS NPLs prepared with c-ALD (black squares) and the current route at 100–150 °C (blue triangles). The horizontal error bars represent the standard deviation of the shell thickness (SI, Figure S6). For comparison, a ZnS shell was grown on CdSe QDs using c-ALD (red dots). Results are also compared to CdSe/CdS NPLs, synthesized with c-ALD, and *k·p* calculations of the CdSe/ZnS exciton energy (open circles). (b) HAADF-STEM image showing a bending of CdSe/ZnS NPLs with a 16 ML shell. (c) Fourier-filtered HR-TEM image of CdSe/ZnS NPLs with a 2 ML shell, with a tilting of 10° of the ZnS lattice relative to the CdSe core.

excluded in both procedures. The results are not unique to 2D NPLs, as CdSe/ZnS QDs, synthesized using c-ALD and with a targeted thickness of up to 8 ML, also yielded a red shift of 35 nm (Figure 6, red dots, and SI, Figure S10). The smaller value obtained for QDs, however, highlights the advantage of 2D NPLs for tuning the band gap and PL spectrum over a wide range via a type-I ZnS shell.

While a quantitative description is beyond the scope of the current article, we can note some factors that may contribute to the red shift of the CdSe/ZnS band-edge absorption and emission. First, considering that the CdSe/ZnS NPLs show a strong red shift already when adding a single layer of S (see also SI, Figure S8b), results suggest that, despite the type-I band alignment, the strong exciton confinement induced in 1.2 nm thick NPLs leads to an exciton delocalization into the ZnS shell and thus reduced quantum confinement along the transversal direction. Second, the PL red shift may be further induced by dielectric screening effects from the shell/ligand interface, leading to a reduction of the electron and hole self-energy.[49]

A calculation of the exciton confinement energy as a function of the ZnS shell growth confirmed these trends. Within the framework of single-band *k·p* theory, we numerically calculated the electron and hole confinement energies and wave functions in the transversal direction, taking into account the finite CdSe/ZnS band offset and the Coulomb self-polarization contribution that stems from the NPL/ligand dielectric contrast.[50] Then, following a variational procedure (see SI, theoretical section), we obtained the in-plane contributions to the exciton energy and wave function. These included the polarization of the Coulomb interaction owing to the dielectric mismatch[50] and the effects of the reduced dimensionality of the CdSe NPLs on the electron and hole effective masses.[49] The calculations yielded an electron and hole wave function tunneling into the ZnS shell (SI, Figure S11e) and a consequent red shift of the emission wavelength with increasing shell thickness, in agreement with the experimental findings (Figure 6a, open circles). The larger magnitude of the red shift as compared to the CdSe/ZnS QDs (Figure 6, dots) can be mainly ascribed to the 1.2 nm NPL thickness. Despite the large CdSe/ZnS band offset, the strong confinement in this dimension increases significantly the single particle band gap, promoting tunneling of the electron and hole into the shell. A more thorough analysis revealed, however, that the delocalization of the exciton into the ZnS shell is not sufficient to account for the strong PL red shift (SI, Figure S11a). We found that the discontinuity of the dielectric screening at the NPLs surface further influences the electron and hole wave functions and associated exciton energy (SI, Figure S11d), giving rise to (i) a notable increase of the calculated red shifts for each ZnS shell thickness, and (ii) an enhanced electron–hole correlation. Both effects stem from the extreme anisotropy of the NPL geometry. In the first case, such anisotropy hinders the mutual compensation of surface polarization and self-polarization terms, extensively reported for excitons in QDs.[56−59] This distinctive feature of NPLs explains their stronger PL red shift after shell growth as compared to QDs. Indeed, in NPLs, the attraction of the electron and hole image charges compensates only partially the dominating repulsive effect of single-particle self-energies.[60] The difference between these contributions decreases when the extreme anisotropy of the dielectric confinement is relieved by growing the ZnS shell and moving the NPL–ligands dielectric interface further out. The overall effect is a reduction of the (net) repulsive contribution of the dielectric effects as the ZnS shell grows thicker, and a concomitant PL red shift. In the second case, the weak in-plane confinement turns the exciton wave function very reactive against changes in the electron–hole interaction potential, which is highly influenced by the strong dielectric confinement in the transversal direction. The immediate consequences are large electron–hole overlaps (SI, Figure S11b–d) and thus short PL lifetimes. In this regard, the calculations predict a decrease of the overlap, up to 50%, as a function of the shell thickness (SI, Figure S11b), which is a direct consequence of relaxing the transversal dielectric confinement. The calculations were corroborated by a measurement of the PL decay trace of samples with varying shell thickness (SI, Figure S7 and Table S2). In line with the reduced electron–hole overlap, after ZnS shell growth we observed an extension of the average PL decay time.

Finally, as already suggested by the XRD and HR-TEM data, due to the 1.2 nm CdSe NPL thickness and the large lattice mismatch between CdSe and ZnS, strain may also build up inside the CdSe core. The presence of strain in our structures is further apparent from a HAADF-STEM image for CdSe/ZnS core/shell NPLs (Figure 6b), where we observed a bending of the CdSe/ZnS NPLs. Moreover, Fourier-filtered HR-TEM images (Figure 6c, CdSe/ZnS with a 2 ML ZnS shell) demonstrate that the CdSe and ZnS [100] crystal directions are slightly misaligned. These strain-induced CdSe lattice modifications and overall bending of the NPLs may cause a further correction to the PL red shift, the latter similar to the reduction

DOI: 10.1021/acs.chemmater.7b01513
Chem. Mater. 2017, 29, 5671–5680

of the band edge already observed in elastically bent CdS nanowires.[61]

Next to the results presented above, the shell growth procedure can also be expanded to CdS and CdZnS shells. For instance, a CdS shell can be grown in toluene at 100−110 °C, using only $CdCl_2$ and equimolar amount of CS_2 in the presence of TOP (SI, Figure S12). As the valence band offset is strongly reduced in CdSe/CdS core/shell NPLs, these samples displayed a significant red shift of the PL maximum, up to 620 nm when targeting a shell thickness of 6 ML (in line with the large red shift observed when applying a CdS shell by c-ALD, Figure 6, green diamonds). However, when growing the shell with this procedure, CdS also nucleated on the edges of the CdSe NPLs as small clusters (SI, Figure S12c). When applying a continuous injection synthesis in DCB at 150 °C to deposit a CdS shell using also $Cd(DDTC)_2$, these clusters progressed into thin CdS nanorods around the CdSe NPL edges (SI, Figure S12d), similar to previously published results on 2D nanocrystals.[62]

The best results were achieved by exchanging $CdCl_2$ for $ZnCl_2$ while keeping $Cd(DDTC)_2$ as the CdS single-source precursor (at a Cd:Zn ratio of 1:1). Applying again the continuous injection in DCB, we observed a stronger red shift of the PL compared to CdSe/ZnS NPLs (Figure 7), despite the inclusion of $ZnCl_2$ in the synthesis. The PL QE of these samples was raised to 58%. More importantly, the shell was deposited more homogeneously over the CdSe core (Figure 7a), possibly due to the reduced reactivity of $ZnCl_2$ compared to $CdCl_2$, yielding a more controlled growth.

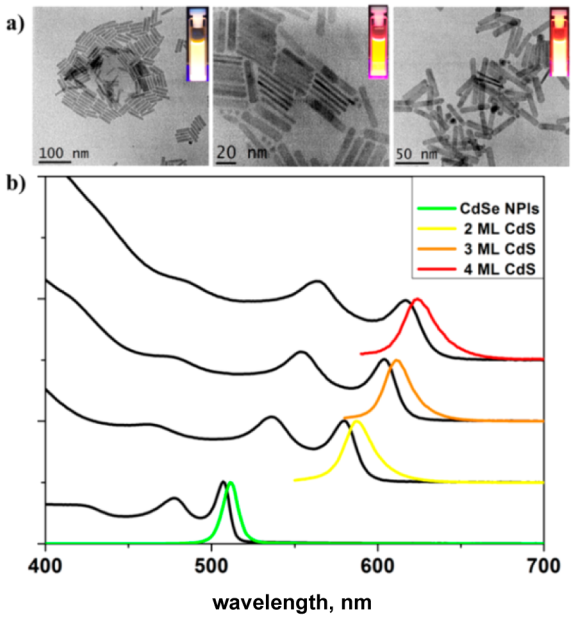

Figure 7. (a) TEM images of CdSe/CdZnS core−shell NPLs with a targeted thickness of 2, 3, and 4 ML, using $ZnCl_2$ and $Cd(DDTC)_2$. The inset shows the NPL dispersion under UV illumination. (b) Corresponding absorbance and photoluminescence spectra.

CONCLUSIONS

We demonstrated a robust procedure for coating CdSe NPLs with ZnS, CdS, and CdZnS, using toluene or DCB as a solvent. The procedure relies on a room temperature injection of precursors followed by heat up or by slow precursor injection at elevated temperatures, and the entire shell growth was performed under open air conditions, demonstrating that synthesis under N_2 atmosphere is not required to obtain high-quality core/shell NPLs. Consequently, it should lend itself well to scale-up. HAAFD-STEM images yielded CdSe/ZnS NPLs with a shell thickness up to 9 ML. Our method yielded CdSe/ZnS and CdSe/CdZnS NPLs with a PL QE up to 64% and 58%, respectively. Despite the type-I band alignment in CdSe/ZnS core−shell NPLs, we observed a significant red shift after shell growth, which could be attributed to exciton delocalization into the ZnS due to strong vertical confinement in 1.2 nm thick CdSe NPLs, as well as a modification of the Coulomb interactions that reduces the electron and hole self-energy. The final samples show excellent stability under ambient conditions, which opens up the way toward practical photonic and optoelectronic applications of CdSe-based 2D NPLs.

ASSOCIATED CONTENT

Supporting Information

The Supporting Information is available free of charge on the ACS Publications website at DOI: 10.1021/acs.chemmater.7b01513.

Absorption and PL spectra of CdSe core and CdSe/ZnS core/shell QDs. Optical spectra and TEM image of CdSe core NPLs. Additional optical spectra of CdSe/ZnS NPLs synthesized by present procedure and room temperature c-ALD. Absorbance spectra of precursors. PL QEs of different CdSe/ZnS NPL samples. Additional details of the *k·p* calculations and plots of the exciton wave function. Additional optical spectra and TEM images for the CdSe/CdS NPLs (PDF)

AUTHOR INFORMATION

Corresponding Author

*E-mail: iwan.moreels@iit.it.

ORCID

Ali Hossain Khan: 0000-0001-7155-0200

Iwan Moreels: 0000-0003-3998-7618

Present Address

[‖]CEA Saclay, 91191 Gif-sur-Yvette, France.

Author Contributions

The manuscript was written through contributions of all authors. All authors have given approval to the final version of the manuscript.

Funding

The present publication is realized with the support of the Ministero degli Affari Esteri e della Cooperazione Internazionale (IONX-NC4SOL). This project has also received funding from the European Union's Horizon 2020 research and innovation program under Grant Agreement No. 696656 (GrapheneCore1). J.L.M. acknowledges support from UJI project P1-1B2014-24 and MINECO project CTQ2014-60178-P.

Notes

The authors declare no competing financial interest.

ACKNOWLEDGMENTS

We thank J. I. Climente and J. Planelles (University Jaume I, Spain) for fruitful discussions.

DOI: 10.1021/acs.chemmater.7b01513
Chem. Mater. 2017, 29, 5671−5680

REFERENCES

(1) Yoffe, A. D. Low-Dimensional Systems: Quantum Size Effects and Electronic Properties of Semiconductor Microcrystallites (Zero-Dimensional Systems) and Some Quasi-Two-Dimensional Systems. *Adv. Phys.* **1993**, *42*, 173−262.

(2) Yin, Y.; Alivisatos, A. P. Colloidal Nanocrystal Synthesis and the Organic-Inorganic Interface. *Nature* **2005**, *437*, 664−670.

(3) Kovalenko, M. V.; Manna, L.; Cabot, A.; Hens, Z.; Talapin, D. V.; Kagan, C. R.; Klimov, V. I.; Rogach, A. L.; Reiss, P.; Milliron, D. J.; Guyot-Sionnnest, P.; Konstantatos, G.; Parak, W. J.; Hyeon, T.; Korgel, B. A.; Murray, C. B.; Heiss, W. Prospects of Nanoscience with Nanocrystals. *ACS Nano* **2015**, *9*, 1012−1057.

(4) Lo, S. S.; Mirkovic, T.; Chuang, C.-H.; Burda, C.; Scholes, G. D. Emergent Properties Resulting from Type-II Band Alignment in Semiconductor Nanoheterostructures. *Adv. Mater.* **2011**, *23*, 180−197.

(5) Fernée, M. J.; Tamarat, P.; Lounis, B. Spectroscopy of Single Nanocrystals. *Chem. Soc. Rev.* **2014**, *43*, 1311−1337.

(6) Kambhampati, P. Multiexcitons in Semiconductor Nanocrystals: A Platform for Optoelectronics at High Carrier Concentration. *J. Phys. Chem. Lett.* **2012**, *3*, 1182−1190.

(7) Pietryga, J. M.; Park, Y.-S.; Lim, J.; Fidler, A. F.; Bae, W. K.; Brovelli, S.; Klimov, V. I. Spectroscopic and Device Aspects of Nanocrystal Quantum Dots. *Chem. Rev.* **2016**, *116*, 10513−10622.

(8) Kagan, C. R.; Lifshitz, E.; Sargent, E. H.; Talapin, D. V. Building Devices from Colloidal Quantum Dots. *Science* **2016**, *353*, aac5523.

(9) Grim, J. Q.; Manna, L.; Moreels, I. A Sustainable Future for Photonic Colloidal Nanocrystals. *Chem. Soc. Rev.* **2015**, *44*, 5897−5914.

(10) Dai, X.; Zhang, Z.; Jin, Y.; Niu, Y.; Cao, H.; Liang, X.; Chen, L.; Wang, J.; Peng, X. Solution-Processed, High-Performance Light-Emitting Diodes Based on Quantum Dots. *Nature* **2014**, *515*, 96−99.

(11) Carey, G. H.; Abdelhady, A. L.; Ning, Z.; Thon, S. M.; Bakr, O. M.; Sargent, E. H. Colloidal Quantum Dot Solar Cells. *Chem. Rev.* **2015**, *115*, 12732−12763.

(12) Saran, R.; Curry, R. J. Lead Sulphide Nanocrystal Photodetector Technologies. *Nat. Photonics* **2016**, *10*, 81−92.

(13) Zhou, J.; Yang, Y.; Zhang, C. Toward Biocompatible Semiconductor Quantum Dots: From Biosynthesis and Bioconjugation to Biomedical Application. *Chem. Rev.* **2015**, *115*, 11669−11717.

(14) Hines, M. A.; Guyot-Sionnest, P. Synthesis and Characterization of Strongly Luminescing ZnS-Capped CdSe Nanocrystals. *J. Phys. Chem.* **1996**, *100*, 468−471.

(15) Talapin, D. V.; Mekis, I.; Götzinger, S.; Kornowski, A.; Benson, O.; Weller, H. CdSe/CdS/ZnS and CdSe/ZnSe/ZnS Core−Shell−Shell Nanocrystals. *J. Phys. Chem. B* **2004**, *108*, 18826−18831.

(16) Mahler, B.; Spinicelli, P.; Buil, S.; Quelin, X.; Hermier, J.-P.; Dubertret, B. Towards Non-Blinking Colloidal Quantum Dots. *Nat. Mater.* **2008**, *7*, 659−664.

(17) Chen, Y.; Vela, J.; Htoon, H.; Casson, J. L.; Werder, D. J.; Bussian, D. A.; Klimov, V. I.; Hollingsworth, J. A. Giant" Multishell CdSe Nanocrystal Quantum Dots with Suppressed Blinking. *J. Am. Chem. Soc.* **2008**, *130*, 5026−5027.

(18) Bae, W. K.; Padilha, L. A.; Park, Y.-S.; McDaniel, H.; Robel, I.; Pietryga, J. M.; Klimov, V. I. Controlled Alloying of the Core−Shell Interface in CdSe/CdS Quantum Dots for Suppression of Auger Recombination. *ACS Nano* **2013**, *7*, 3411−3419.

(19) Christodoulou, S.; Vaccaro, G.; Pinchetti, V.; de Donato, F.; Grim, J. Q.; Casu, A.; Genovese, A.; Vicidomini, G.; Diaspro, A.; Brovelli, S.; Manna, L.; Moreels, I. Synthesis of Highly Luminescent Wurtzite CdSe/CdS Giant-Shell Nanocrystals Using a Fast Continuous Injection Route. *J. Mater. Chem. C* **2014**, *2*, 3439−3447.

(20) Ithurria, S.; Tessier, M. D.; Mahler, B.; Lobo, R. P. S. M.; Dubertret, B.; Efros, A. L. Colloidal Nanoplatelets with Two-Dimensional Electronic Structure. *Nat. Mater.* **2011**, *10*, 936−941.

(21) Lhuillier, E.; Pedetti, S.; Ithurria, S.; Nadal, B.; Heuclin, H.; Dubertret, B. Two-Dimensional Colloidal Metal Chalcogenides Semiconductors: Synthesis, Spectroscopy, and Applications. *Acc. Chem. Res.* **2015**, *48*, 22−30.

(22) Zhang, F.; Wang, S.; Wang, L.; Lin, Q.; Shen, H.; Cao, W.; Yang, C.; Wang, H.; Yu, L.; Du, Z.; Xue, J.; Li, L. S. Super Color Purity Green Quantum Dot Light-Emitting Diodes Fabricated by Using CdSe/CdS Nanoplatelets. *Nanoscale* **2016**, *8*, 12182−12188.

(23) Naeem, A.; Masia, F.; Christodoulou, S.; Moreels, I.; Borri, P.; Langbein, W. Giant Exciton Oscillator Strength and Radiatively Limited Dephasing in Two-Dimensional Platelets. *Phys. Rev. B: Condens. Matter Mater. Phys.* **2015**, *91*, 121302.

(24) Achtstein, A. W.; Schliwa, A.; Prudnikau, A.; Hardzei, M.; Artemyev, M. V.; Thomsen, C.; Woggon, U. Electronic Structure and Exciton−Phonon Interaction in Two-Dimensional Colloidal CdSe Nanosheets. *Nano Lett.* **2012**, *12*, 3151−3157.

(25) She, C.; Fedin, I.; Dolzhnikov, D. S.; Demortière, A.; Schaller, R. D.; Pelton, M.; Talapin, D. V. Low-Threshold Stimulated Emission Using Colloidal Quantum Wells. *Nano Lett.* **2014**, *14*, 2772−2777.

(26) Grim, J. Q.; Christodoulou, S.; Di Stasio, F.; Krahne, R.; Cingolani, R.; Manna, L.; Moreels, I. Continuous-Wave Biexciton Lasing at Room Temperature Using Solution-Processed Quantum Wells. *Nat. Nanotechnol.* **2014**, *9*, 891−895.

(27) Guzelturk, B.; Kelestemur, Y.; Olutas, M.; Delikanli, S.; Demir, H. V. Amplified Spontaneous Emission and Lasing in Colloidal Nanoplatelets. *ACS Nano* **2014**, *8*, 6599−6605.

(28) Li, M.; Zhi, M.; Zhu, H.; Wu, W.-Y.; Xu, Q.-H.; Jhon, M. H.; Chan, Y. Ultralow-Threshold Multiphoton-Pumped Lasing from Colloidal Nanoplatelets in Solution. *Nat. Commun.* **2015**, *6*, 8513.

(29) She, C.; Fedin, I.; Dolzhnikov, D. S.; Dahlberg, P. D.; Engel, G. S.; Schaller, R. D.; Talapin, D. V. Red, Yellow, Green, and Blue Amplified Spontaneous Emission and Lasing Using Colloidal CdSe Nanoplatelets. *ACS Nano* **2015**, *9*, 9475−9485.

(30) Kelestemur, Y.; Guzelturk, B.; Erdem, O.; Olutas, M.; Gungor, K.; Demir, H. V. Platelet-in-Box Colloidal Quantum Wells: CdSe/CdS@CdS Core/Crown@Shell Heteronanoplatelets. *Adv. Funct. Mater.* **2016**, *26*, 3570−3579.

(31) Tessier, M. D.; Mahler, B.; Nadal, B.; Heuclin, H.; Pedetti, S.; Dubertret, B. Spectroscopy of Colloidal Semiconductor Core/Shell Nanoplatelets with High Quantum Yield. *Nano Lett.* **2013**, *13*, 3321−3328.

(32) Flatten, L. C.; Christodoulou, S.; Patel, R. K.; Buccheri, A.; Coles, D. M.; Reid, B. P. L.; Taylor, R. A.; Moreels, I.; Smith, J. M. Strong Exciton−Photon Coupling with Colloidal Nanoplatelets in an Open Microcavity. *Nano Lett.* **2016**, *16*, 7137−7141.

(33) Jana, S.; Davidson, P.; Abécassis, B. CdSe Nanoplatelets: Living Polymers. *Angew. Chem., Int. Ed.* **2016**, *55*, 9371−9374.

(34) Abécassis, B.; Tessier, M. D.; Davidson, P.; Dubertret, B. Self-Assembly of CdSe Nanoplatelets into Giant Micrometer-Scale Needles Emitting Polarized Light. *Nano Lett.* **2014**, *14*, 710−715.

(35) Rowland, C. E.; Fedin, I.; Zhang, H.; Gray, S. K.; Govorov, A. O.; Talapin, D. V.; Schaller, R. D. Picosecond Energy Transfer and Multiexciton Transfer Outpaces Auger Recombination in Binary CdSe Nanoplatelet Solids. *Nat. Mater.* **2015**, *14*, 484−489.

(36) Moreels, I. Colloidal Nanoplatelets: Energy Transfer Is Speeded up in 2D. *Nat. Mater.* **2015**, *14*, 464−465.

(37) Prudnikau, A.; Chuvilin, A.; Artemyev, M. CdSe−CdS Nanoheteroplatelets with Efficient Photoexcitation of Central CdSe Region through Epitaxially Grown CdS Wings. *J. Am. Chem. Soc.* **2013**, *135*, 14476−14479.

(38) Li, Q.; Wu, K.; Chen, J.; Chen, Z.; McBride, J. R.; Lian, T. Size-Independent Exciton Localization Efficiency in Colloidal CdSe/CdS Core/Crown Nanosheet Type-I Heterostructures. *ACS Nano* **2016**, *10*, 3843−3851.

(39) Pedetti, S.; Ithurria, S.; Heuclin, H.; Patriarche, G.; Dubertret, B. Type-II CdSe/CdTe Core/Crown Semiconductor Nanoplatelets. *J. Am. Chem. Soc.* **2014**, *136*, 16430−16438.

(40) Mahler, B.; Nadal, B.; Bouet, C.; Patriarche, G.; Dubertret, B. Core/shell Colloidal Semiconductor Nanoplatelets. *J. Am. Chem. Soc.* **2012**, *134*, 18591−18598.

(41) Ithurria, S.; Talapin, D. V. Colloidal Atomic Layer Deposition (c-ALD) Using Self-Limiting Reactions at Nanocrystal Surface

DOI: 10.1021/acs.chemmater.7b01513
Chem. Mater. 2017, 29, 5671−5680

Coupled to Phase Transfer between Polar and Nonpolar Media. *J. Am. Chem. Soc.* **2012**, *134*, 18585−18590.
(42) Lorenzon, M.; Christodoulou, S.; Vaccaro, G.; Pedrini, J.; Meinardi, F.; Moreels, I.; Brovelli, S. Reversed Oxygen Sensing Using Colloidal Quantum Wells towards Highly Emissive Photoresponsive Varnishes. *Nat. Commun.* **2015**, *6*, 6434.
(43) Pradhan, N.; Katz, B.; Efrima, S. Synthesis of High-Quality Metal Sulfide Nanoparticles from Alkyl Xanthate Single Precursors in Alkylamine Solvents. *J. Phys. Chem. B* **2003**, *107*, 13843−13854.
(44) Chen, D.; Zhao, F.; Qi, H.; Rutherford, M.; Peng, X. Bright and Stable Purple/Blue Emitting CdS/ZnS Core/Shell Nanocrystals Grown by Thermal Cycling Using a Single-Source Precursor. *Chem. Mater.* **2010**, *22*, 1437−1444.
(45) Jung, Y. K.; Kim, J. I.; Lee, J.-K. Thermal Decomposition Mechanism of Single-Molecule Precursors Forming Metal Sulfide Nanoparticles. *J. Am. Chem. Soc.* **2010**, *132*, 178−184.
(46) Bertrand, G. H. V.; Polovitsyn, A.; Christodoulou, S.; Khan, A. H.; Moreels, I. Shape Control of Zincblende CdSe Nanoplatelets. *Chem. Commun.* **2016**, *52*, 11975−11978.
(47) Achtstein, A. W.; Antanovich, A.; Prudnikau, A.; Scott, R.; Woggon, U.; Artemyev, M. Linear Absorption in CdSe Nanoplates: Thickness and Lateral Size Dependency of the Intrinsic Absorption. *J. Phys. Chem. C* **2015**, *119*, 20156−20161.
(48) Hÿtch, M. J.; Snoeck, E.; Kilaas, R. Quantitative Measurement of Displacement and Strain Fields from HREM Micrographs. *Ultramicroscopy* **1998**, *74*, 131−146.
(49) Benchamekh, R.; Gippius, N. A.; Even, J.; Nestoklon, M. O.; Jancu, J.-M.; Ithurria, S.; Dubertret, B.; Efros, A. L.; Voisin, P. Tight-Binding Calculations of Image-Charge Effects in Colloidal Nanoscale Platelets of CdSe. *Phys. Rev. B: Condens. Matter Mater. Phys.* **2014**, *89*, 35307.
(50) Kumagai, M.; Takagahara, T. Excitonic and Nonlinear-Optical Properties of Dielectric Quantum-Well Structures. *Phys. Rev. B: Condens. Matter Mater. Phys.* **1989**, *40*, 12359−12381.
(51) Purdy, A. P.; George, C. F. Anhydrous Dithiocarbamates. Potential Precursors to Alkaline Earth Sulfide Materials. *Main Group Chem.* **1996**, *1*, 229−240.
(52) Zhou, Y.; Wang, F.; Buhro, W. E. Large Exciton Energy Shifts by Reversible Surface Exchange in 2D II−VI Nanocrystals. *J. Am. Chem. Soc.* **2015**, *137*, 15198−15208.
(53) Bianchini, C.; Meli, A.; Orlandini, A. Reactivity of the Triethylphosphine-Carbon Disulfide Adduct (Et3P.CS2) toward cobalt(II) Cations in the Presence of the Tris (Tertiary Phosphines) Triphos and Etriphos. X-Ray Crystal Structure of the Complex [(etriphos)Co(S2C(H)PEt3)](BPh4)2. *Inorg. Chem.* **1982**, *21*, 4161−4165.
(54) Chen, D.; Gao, Y.; Chen, Y.; Ren, Y.; Peng, X. Structure Identification of Two-Dimensional Colloidal Semiconductor Nanocrystals with Atomic Flat Basal Planes. *Nano Lett.* **2015**, *15*, 4477−4482.
(55) Madelung, O., Rössler, U., Schulz, M., Eds. *II-VI and I-VII Compounds; Semimagnetic Compounds*; Landolt-Börnstein: Group III Condensed Matter; Springer-Verlag: Berlin/Heidelberg, 1999; Vol. *41B*.
(56) Brus, L. E. Electron−electron and Electron-hole Interactions in Small Semiconductor Crystallites: The Size Dependence of the Lowest Excited Electronic State. *J. Chem. Phys.* **1984**, *80*, 4403−4409.
(57) Lannoo, M.; Delerue, C.; Allan, G. Screening in Semiconductor Nanocrystallites and Its Consequences for Porous Silicon. *Phys. Rev. Lett.* **1995**, *74*, 3415−3418.
(58) Bolcatto, P. G.; Proetto, C. R. Shape and Dielectric Mismatch Effects in Semiconductor Quantum Dots. *Phys. Rev. B: Condens. Matter Mater. Phys.* **1999**, *59*, 12487−12498.
(59) Fonoberov, V. A.; Pokatilov, E. P.; Balandin, A. A. Exciton States and Optical Transitions in Colloidal CdS Quantum Dots: Shape and Dielectric Mismatch Effects. *Phys. Rev. B: Condens. Matter Mater. Phys.* **2002**, *66*, 85310.
(60) Rodina, A. V.; Efros, A. L. Effect of Dielectric Confinement on Optical Properties of Colloidal Nanostructures. *J. Exp. Theor. Phys.* **2016**, *122*, 554−566.
(61) Zhang, C.; Cretu, O.; Kvashnin, D. G.; Kawamoto, N.; Mitome, M.; Wang, X.; Bando, Y.; Sorokin, P. B.; Golberg, D. Statistically Analyzed Photoresponse of Elastically Bent CdS Nanowires Probed by Light-Compatible In Situ High-Resolution TEM. *Nano Lett.* **2016**, *16*, 6008−6013.
(62) Wu, X.-J.; Chen, J.; Tan, C.; Zhu, Y.; Han, Y.; Zhang, H. Controlled Growth of High-Density CdS and CdSe Nanorod Arrays on Selective Facets of Two-Dimensional Semiconductor Nanoplates. *Nat. Chem.* **2016**, *8*, 470−475.

DOI: 10.1021/acs.chemmater.7b01513
Chem. Mater. 2017, 29, 5671−5680